

The nature of the charge density waves in under-doped $\text{YBa}_2\text{Cu}_3\text{O}_{6.54}$ revealed by X-ray measurements of the ionic displacements

E. M. Forgan¹, E. Blackburn¹, A.T. Holmes¹, A. Briffa¹, J. Chang², L. Bouchenoire^{3,4}, S.D. Brown^{3,4}, Ruixing Liang⁵, D. Bonn⁵, W. N. Hardy⁵, N. B. Christensen⁶, M. v. Zimmermann⁷, M. Hücker⁸ and S.M. Hayden⁹

¹School of Physics & Astronomy, University of Birmingham, Birmingham B15 2TT, UK

²Physik-Institut, Universität Zürich, Winterthurerstrasse 190, CH-8057 Zürich, Switzerland

³XMaS, European Synchrotron Radiation Facility, B. P. 220, F-38043 Grenoble Cedex, France

⁴Department of Physics, University of Liverpool, Liverpool, L69 3BX, UK

⁵Department of Physics & Astronomy, University of British Columbia, Vancouver, Canada

⁶Department of Physics, Technical University of Denmark, DK-2800 Kongens Lyngby, Denmark

⁷Deutsches Elektronen-Synchrotron DESY, 22603 Hamburg, Germany

⁸Condensed Matter Physics & Materials Science Department, Brookhaven National Laboratory, Upton, New York 11973, USA

⁹H. H. Wills Physics Laboratory, University of Bristol, Bristol, BS8 1TL, UK

Underdoped high-temperature cuprate superconductors now appear to ubiquitously exhibit charge density wave (CDW) order. For hole doping near 1/8 per planar copper atom, the CDW order develops above the superconducting transition temperature, T_c , and competes with the superconductivity below T_c . Experiments show that the modulations of the CDW order are aligned with both CuO directions in the CuO_2 planes with a period of 3-5 lattice spacings. However, the microscopic

symmetry breaking corresponding to the CDW order has remained unclear. Here we use X-ray diffraction to determine the ionic displacements associated with the CDW order in the archetypical material $\text{YBa}_2\text{Cu}_3\text{O}_{7-x}$ (YBCO). We find that major components of the CDW are *shear* displacements perpendicular to the CuO_2 planes. These remove the mirror symmetry of the CuO_2 bilayers and have important implications for understanding the signals from other probes of the CDW order. For example, our results for the copper and oxygen displacement patterns give an explicit explanation of how signals described as “*s*- and/or bond *d*-density waves” can appear in scanning tunnelling microscopy (STM) and soft X-ray measurements. The CDW symmetry that we discover has implications for Fermi surface reconstruction observed by quantum oscillation (QO) measurements. Finally, we measure the *a/b* anisotropy of the CDWs and find that the amplitudes of the *a* and *b*-axis components are of the same order.

Introduction

The story of CDWs in High- T_c materials (other than the ‘214’ compounds related to $(\text{La/Ba})_2\text{CuO}_4$ which show “stripe” behaviour¹) started with Quantum Oscillation (QO) measurements that showed unexpectedly small Fermi surface (FS) pockets² and transport measurements that indicated a change from hole carriers in the over-doped region and at high temperatures to electron-like transport in the under-doped region at low temperatures³. Nuclear magnetic resonance (NMR) measurements on under-doped YBCO⁴ gave clear indications of charge density waves, stimulating a search for diffraction evidence for a broken translational symmetry that might explain FS reconstruction. Charge density modulations were initially observed in YBCO by diffraction using two primary techniques. The first of these, resonant soft X-ray scattering at a Cu *L*-edge⁵⁻⁸, is particularly sensitive to small modulations in the *L*-edge resonance energies of the *d*-electrons in chain and planar Cu ions⁶. This sensitivity, and the polarisation-dependence

of the signal, have been used to indicate that the major part of the charge density modulation is localized near the planar Cu ions only⁶. However, this technique can only examine a limited portion of reciprocal space, due to the long wavelength of X-rays at the Cu *L*-edges ($\sim 15 \text{ \AA}$). To access a larger volume of reciprocal space, higher X-ray energies must be used, but then the scattering is non-resonant. Therefore, all of the ions in the unit cell contribute to the observed scattering, particularly the more massive ones carrying many electrons. Such measurements were originally carried out at X-ray energies $\geq 80 \text{ keV}$, and showed that the CDW displacements in adjacent unit cells in the *c*-direction are in antiphase⁹⁻¹¹.

Charge density waves occur in many metals (see ref. 12 for a recent review). Some of the most well-known examples are the transition metal chalcogenides, such as *2H*-NbSe₂ and TaSe₂ (ref. 13). A classic charge density wave is a periodic modulation of the electron density, and is typically associated with a periodic lattice distortion (this may or may not be commensurate with the crystal lattice). The electron (or charge) density modulation may be brought about by electron-phonon or electron-electron interactions¹⁴.

It has become clear that the CDW state is a ubiquitous High-*T_c* phenomenon. It has now been observed in Bi₂Sr_{2-x}La_xCuO_{6+x}¹⁵, Bi₂Sr₂CaCu₂O_{8+x}¹⁶, Bi_{1.5}Pb_{0.6}Sr_{1.54}CaCu₂O_{8+x}¹⁷, La_{2-x}Sr_xCuO₄¹⁸ and HgBa₂CuO_{4+x}¹⁹, using Cu *L*-edge resonant X-ray scattering, and in La_{2-x}Sr_xCuO₄ using high energy X-rays^{20,21}. More detailed experiments on YBCO using soft X-rays suggest a *d*-wave symmetry for charges on the oxygen bonds around the Cu site²², as suggested by Sachdev²³. This conclusion has been supported by scanning tunnelling microscopy (STM) observations of the surface of Bi₂Sr₂CaCu₂O_{8+x} and Ca_{2-x}Na_xCuO₂Cl₂²⁴, although further soft X-ray measurements²⁵ suggest that the situation in YBCO is more complicated.

It has been proposed²⁶ that these CDWs have a stripe structure similar to that in 214-compounds, i.e. that the ordering is single-**q** (1-**q**) in any given region of the crystal, with modulations associated with the **a** and **b** directions in different regions. However, ultrasonic measurements of the *c*₆₆ elastic modulus at high fields and low temperatures in YBCO²⁷ show clearly that the CDW order is double-**q** (2-**q**) with *both* modulations present in the same region. This conclusion is strengthened by QO measurements^{19,28,29}, which rely on the existence of 2-**q** CDW ordering to interpret the FS reconstruction. However, the field and temperature region where QO measurements are made appears to be bounded by a 2nd-order phase

transition²⁷, so the question arises whether the CDW order is also $2\text{-}\mathbf{q}$ at lower fields and higher temperatures. The transition between fully-developed pre-existing $1\text{-}\mathbf{q}$ order and $2\text{-}\mathbf{q}$ order cannot be continuous due to the nature of the symmetry breaking, suggesting that the order observed at lower fields and higher temperatures is also $2\text{-}\mathbf{q}$. In addition, the signs of FS reconstruction in transport measurements extend to lower fields and higher temperatures³.

The similarity of the results for the \mathbf{a} and \mathbf{b} directions in the present paper, and their similar temperature dependence also argue for the $2\text{-}\mathbf{q}$ scenario. The basal-plane coherence of the CDW order is quite short, probably representing the effect of pinning. Recently it has been argued³⁰ that the different anisotropy of the coherence lengths for the two \mathbf{q} s implies that they must arise in different domains and therefore the CDW structure is stripe-like i.e. $1\text{-}\mathbf{q}$. However this argument is only valid if the coherence length arises from the finite size of domains, and does not apply if the coherence length arises from pinning that is *anisotropic with respect to \mathbf{q}* for each of the two CDW wavevectors present in the same region. It is found that the coherence lengths change with temperature and magnetic field⁹, but not enough to conclude that the CDW occupies small regions of the sample which then grow in size. We shall therefore assume that $2\text{-}\mathbf{q}$ CDW order is present throughout the whole crystal. This only affects numerical estimates of the magnitude of the displacements; all qualitative features of the CDW components are independent of this assumption.

In this experiment, we use mid-range 14 keV non-resonant X-ray diffraction to measure the intensities of ~ 200 different CDW satellites with both modulation vectors $\mathbf{q}_a = (\delta_a, 0, 0.5)$ and $\mathbf{q}_b = (0, \delta_b, 0.5)$. Here, $\delta_a \sim 0.323$, $\delta_b \sim 0.328$ for our under-doped YBCO crystal with ortho-II structure (oxygen site in alternate CuO chains unoccupied). Throughout the paper, we express wavevectors in reciprocal space coordinates (h, k, ℓ) , where $\mathbf{Q} = (h\mathbf{a}^* + k\mathbf{b}^* + \ell\mathbf{c}^*)$; \mathbf{q} is used to denote the full wavevector of a CDW mode and δ its basal plane part. From the results we deduce the patterns of ionic displacements of the ions in the unit cell; these reveal important new aspects of the physics of the CDW.

Experimental results

Non-resonant X-rays are primarily sensitive to the ionic displacements associated with a CDW, rather than changes in charge densities, although if one of these is present, so must the other (see Supplementary Information). The CDW order gives rise to very weak diffraction satellites at positions in reciprocal space $\mathbf{Q} = \boldsymbol{\tau} \pm \mathbf{q}$ around lattice Bragg peaks $\boldsymbol{\tau}$ which are at integer h, k , and ℓ . The variation of the intensities with position in reciprocal space reflects the contributions of the different displacements of ions throughout the unit cell. The key point to note is that the diffraction amplitude at wavevector \mathbf{Q} due to an ion carrying a total of N electrons which is displaced by small distance \mathbf{u} gives an amplitude for CDW diffraction $\sim N \mathbf{Q} \cdot \mathbf{u}$. By observing the intensity of CDW diffraction signals over a wide range of directions and values of \mathbf{Q} we can determine both the amplitude and direction of the displacements of the ions. The full theory relating the CDW satellite intensities to the displacements is given in the Supplementary Information.

To obtain sufficient data required the flexibility of a 4-circle diffractometer, which is provided at the XMaS beamline at the ESRF. The intensities of the \mathbf{q}_a and \mathbf{q}_b satellites in our sample appear at the same temperature (Fig. 1 (d)), suggesting that CDW ordering is a combination of both of them present together. Measurements were made at the superconducting T_c of our sample (60 K), where the CDW intensity is maximised⁹. Details about the sample used are given in ref. 10. Fig. 1 (a-c) shows some typical scans through CDW diffraction satellites. They are found to peak at half-integral values of ℓ (Fig. 1 (e)), and are extremely weak ($\sim 10^{-7}$ of a typical crystal Bragg reflection). Therefore the satellites are measured above a relatively large background, but due to their known position and shape, their intensities can be fitted and spurious signals ignored (see Methods and Supplementary Information).

Ionic displacements obtained from the intensities

Group theory indicates which incommensurately modulated displacement patterns and irreducible representations (IR) are consistent with the observed ordering wavevectors. There are four patterns (IRs) for each ordering wavevector, labelled A_1, A_2, A_3, A_4 for \mathbf{q}_a and similarly $B_1 - B_4$ for \mathbf{q}_b ³¹. The even-

numbered patterns (IRs) have purely basal-plane transverse displacements, and are therefore incompatible with our observations of satellites close to both the \mathbf{c}^* axis and the basal plane⁹. The other patterns (two-dimensional IRs) have longitudinal displacements in the basal plane parallel to δ combined with shear displacements parallel to the \mathbf{c} -axis. Patterns A_3 and B_3 (see Supplementary Information) have equal *longitudinal* displacements in the two halves of a CuO_2 bilayer, which have the yttrium mirror plane of the crystal structure between them. These displacements would be associated with CDW charge density modulations which are equal in the two halves of a bilayer. For these patterns A_3 and B_3 , the yttrium layer is also a mirror plane of the CDW, so the \mathbf{c} -axis shear displacements would be equal and opposite on the two sides of the bilayer. In contrast, the A_1 and B_1 patterns have equal \mathbf{c} -axis *shear* displacements in the two halves of the CuO_2 bilayer region, combined with basal plane compressive displacements and CDW charge density modulations which are equal and opposite on the two sides of the bilayer. For these A_1 and B_1 patterns, the CuO chain layer is a mirror plane of the CDW. In all cases, we may write the displacements \mathbf{u}_j , of the individual ions from their regular positions \mathbf{r}_j^0 as a sum of two terms, one of which is polarised along \mathbf{c} (\mathbf{u}_j^c) and the other (\mathbf{u}_j^a or \mathbf{u}_j^b) parallel to δ , with mirror symmetry about the relevant layer of the crystal.

$$\mathbf{r}_j = \mathbf{r}_j^0 + \mathbf{u}_j^c \cos(\delta \cdot \mathbf{r}_j^0 + \varphi) + \mathbf{u}_j^{a,b} \sin(\delta \cdot \mathbf{r}_j^0 + \varphi), \quad (1)$$

Symmetry³¹ requires that the displacements corresponding to the \mathbf{u}_j^c and $\mathbf{u}_j^{a,b}$ terms are $\pi/2$ out of phase (see Eq. 1). Because the next unit cell along the c -axis is in antiphase, some displacements are zero by symmetry. The models described above all involve 13 nonzero ionic displacement components which can be varied in magnitude and sign to fit the data. We find no evidence for different responses in those cells having a full or empty CuO chain (no CDW satellites are observed about $\tau + \frac{1}{2}\mathbf{a}^*$ positions), so we average over this half-occupied oxygen site in our analysis.

The CDW intensities were fitted using a non-linear least squares fitting program which iterated towards a minimum of χ^2 . When using models A_3 or B_3 , which emphasised longitudinal displacements in the CuO_2 layers, the fit was very poor, as demonstrated for the \mathbf{q}_b mode in the right-hand panel of Fig. 2. Since 13

parameters were available, it was always possible that the program was iterating towards a local rather than a global minimum in χ^2 ; however, using 1.6 million different initial signs/values did not give an improvement of the fit.

In contrast, model B_1 , which gives mainly shear displacements in the CuO_2 layers, always converged in a few iterations to a good fit ($\chi^2(B_1) < \chi^2(B_3) / 10$) and gave the same fitted values of displacements independent of the starting value of the parameters. This leads us to conclude that it is close to an accurate representation of the CDW with modulation vector \mathbf{q}_b . Fitting of the intensity data from the CDW with \mathbf{q}_a gives a very similar pattern of displacements. The \mathbf{q}_a data are somewhat sparser and the results have larger errors (see Supplementary Information). This is due to the tails of the peaks arising from the ortho-II oxygen-ordering giving large and rapidly varying backgrounds.

In Fig. 3, we represent the patterns of ionic displacements in a single unit cell as given by the data for both \mathbf{q}_a and \mathbf{q}_b modulations. The overall similarity of the two CDWs is apparent. To give the spatial variation of the ionic displacements, shown in Fig. 4, the c -axis and basal plane displacements for the \mathbf{q}_a mode are modulated by $\cos(2\pi\delta_a x/a)$ and $\sin(2\pi\delta_a x/a)$ respectively, and similarly for the \mathbf{q}_b mode. The half-modulation period is quite short ($\sim 1\frac{1}{2}$ unit cells), so that the spatial variation of displacements shown in Fig. 4 appears somewhat different from the single unit cell motifs in Fig. 3 from which they are derived.

We note that the coherence length of the CDW is not long enough for the incommensuracy to sample all phases relative to the lattice in a single coherent region (a coherence length of ~ 20 unit cells gives a phase slip of $\sim 0.4 \pi$ for $(\delta_a - 1/3) \sim 0.01$, and $\sim 0.2 \pi$ in for δ_b). The CDW may have a lower energy for a particular phase and hence might accommodate slight incommensuracy (driven by band structure effects) by incorporating defects in the CDW. We cannot obtain the CDW phase relative to the lattice from intensity results (see Supplementary Information) – in appropriate cases this can be done by STM at the surface²⁴.

Discussion

As expected, from the observed competition with superconductivity^{4,5,6,9}, the ionic displacements are maximal near the CuO₂ planes and are weak near the CuO chains. Certain features of our fit, such as the *c*-axis motion of the yttrium layer moving *with* both the CuO₂ planes are expected on physical grounds, but were not imposed as constraints, giving extra confidence in the fit results.

The largest amplitudes are out-of-plane *shear* rather than compression of the CuO₂ planes, so that the CDW is not *purely* a separation of charge as commonly assumed. It may be that the lattice is deforming in this way because shear deformations cost less elastic energy than compressive ones. There are also CDW-modulated charges associated with the small longitudinal displacements in the two halves of a bilayer, but they are equal and opposite: this would be favoured by Coulomb effects within a bilayer. We note the similarity of some of the displacements to a soft phonon observed in optimally doped YBCO³². However, in that mode, the *c*-motion is in *antiphase* for the two halves of the bilayer. Buckling of the CuO₂ planes is also seen in 214 compounds¹, where it mainly consists of tilts of rigid Cu-O octahedra. Here however, the displacements in the CuO₂ layers are clearly inconsistent with tilts of a rigid arrangement of ions.

We draw attention to the up/down “butterfly” nature of the displacements of the four oxygens around the Cu in the bilayers, which is seen for both \mathbf{q}_a and \mathbf{q}_b modes. The pair of oxygens around a copper in the δ -direction has displacements in phase with the Cu and the other perpendicular pair is in antiphase (see Fig. 3). To an STM²⁴ this could appear to be a ‘*d*-charge density’ on the oxygens, since *c*-axis motion of an oxygen – relative to the yttrium and/or to the crystal surface would alter its local doping and electronic state. (The STM measurements are analysed in such a way as to emphasise the electronic states, rather than the positions of atoms.) Are oxygen *c*-axis displacements *simulating* the *d*-density pattern observed on the surface of two other High-*T_c* compounds²⁴? The observed displacements could either be caused by, or give rise to, a *d*-density on the oxygens. However, we incline to the view that the shear of an entire bilayer, with the yttrium displaced in concert with the copper ions is less easy to account for in a pure

bond d -density wave picture, and it would contribute to what has been called an s -density component of the CDW²⁵.

There is an interesting link between the symmetry of the CDW and other measurements. We note that ultrafast excitation of a B_{1u} mode dominated by the c -axis motion of the oxygen atoms leads to a temporary increase in T_c and strongly affects the CDW³³. This is most likely because this phonon mode results in the c -axis motion of the same atoms involved in the CDW distortion, which disrupts the CDW.

We have obtained an estimate of the absolute magnitude of ion displacements by comparing the satellite intensities with Bragg peaks from the lattice, on the assumption that both CDWs occupy the whole of the crystal. The fitted values of the ionic displacements are given in the Supplementary Information. The differences in the magnitudes of the X-ray signals from the \mathbf{q}_a and \mathbf{q}_b modes^{8,10} have suggested that the CDW in o-II YBCO might be essentially single- \mathbf{q} , and dominated by the \mathbf{q}_b mode. Our results indicate that the two modes have similar displacement amplitudes - but the value of their ratio depends on which ion is chosen to make the comparison. For instance, if we take the butterfly motion of the CuO_2 plane oxygens as a key component of the CDW, we find that the *relative* c -motion of these oxygen ions is essentially identical for the two modes: in both cases, the amplitude is $\sim 4\text{-}5 \times 10^{-3}$ Å. Our fits also show differences in the heavy ion displacements, and even if these are small, they can make noticeable contributions to the X-ray signals because they carry many core electrons. Thus, only our complete survey, rather than measurements of the intensities of a few \mathbf{q}_a and \mathbf{q}_b satellites, can reveal the similarities and slight differences between the two CDW modes.

To consider the effects on FS reconstruction, we note that the CDW perturbation may couple a carrier state with momentum (\mathbf{k}, k_z) , where \mathbf{k} is the basal plane momentum, to another at $(\mathbf{k}+\boldsymbol{\delta}, k_z + \pi/c)$ ^{9,29}. If these two states are degenerate, strong hybridisation will occur when the matrix elements of the perturbation are nonzero. The displacements associated with the CDW break the mirror symmetry of the bilayer, and cause opposite perturbations on the carriers on the two halves of a bilayer. The value of a matrix element depends on this symmetry and on that of the bilayer states and the details are discussed in a forthcoming publication³⁴. Fig. 5 shows schematically where the hybridisation may take place and lead

to FS reconstruction. This scenario naturally generates the multiple frequencies observed in QO experiments^{28,29}.

Conclusions and interesting questions remaining

These results carry several important messages. Firstly they show that a strictly “planar” account of High- T_c phenomena may miss important aspects of the physics, and that the 3rd dimension and crystal lattice effects cannot be ignored. In our experiments we have observed a charge density wave which has a strong *shear* (*c*-axis) component. However, the “butterfly” pattern of oxygen shear displacements around the planar copper ions can simulate a *d*-charge density on the oxygens. It will be very interesting to repeat these X-ray measurements on other under-doped High- T_c compounds to establish the generality (or otherwise) of these results. We note that the CDWs in YBCO are nearly commensurate, and may be present in finite domains with a fixed phase of the distortions relative to the crystal lattice. If so, this phase might be established by STM, or detailed modelling of other measurements such as NMR. It will be very interesting to discover what changes in the CDW occur at high fields where quantum oscillation measurements are performed. Ultrasonic measurements²⁷ show that changes occur at about 18 T in this material and that the order is $2\mathbf{q}$. The changes may represent the onset of exact commensuracy, increased coherence lengths, (less likely a change from $1\mathbf{q}$ to $2\mathbf{q}$), or an increase in the amplitude of the CDW. Since diffraction is extremely difficult at > 18 T, the answer to this question may again lie in the modelling of other measurements. We note that to explain the reconstruction of the FS to give a small electron-like surface in the under-doped region, the effects of the CDW must be combined with those of the pseudogap^{28,35}. It is clear that antiferromagnetic order, the CDW, pseudogap and superconductivity are all intertwined, since they all remove electron states near the antinodal regions of the Fermi surface. It appears that there is a quantum critical point underlying the superconducting dome; we trust that our results will help to achieve an over-arching theory relating the relationship of all these phenomena to High- T_c superconductivity.

Methods

The measurements were carried out on a diffractometer using four-circle geometry at the XMaS beamline at the ESRF, Grenoble. The sample was mounted in a closed-cycle cryostat and all measurements were carried out in reflection from the flat c -face of the crystal (of area $\sim 2 \times 2 \text{ mm}^2$) at an X-ray energy of 14 keV. This gives a penetration depth of 25 microns into the sample, so the results are not dominated by surface effects. For CDW intensity measurements, the sample temperature was controlled at T_c to maximise the signal, and it was taken to 150 K to check for spurious signals which did not go to zero. The diffractometer angles were set so that the incoming and detected beams were close to the same angle to the c -face of the crystal, which allowed correction for sample absorption, as described in the Supplementary Information. CDW intensity measurements were carried out near the $(h, 0, \ell)$, $(0, k, \ell)$ and (h, h, ℓ) planes of reciprocal space over as wide a range of h , k and ℓ allowed by the maximum scattering angle, and the avoidance of grazing incidence at low ℓ . CDW peaks were scanned parallel to δ , through positions of the form $\mathbf{Q} = \tau \pm \mathbf{q}$. The intensities of the CDW peaks were established by fitting each scan with a Gaussian of fixed width, with a smoothly-varying cubic polynomial background. By examination of 150 K measurements, or by the χ^2 of the fit, spurious peaks were removed from the list of measured satellites. The resulting list of intensities, weighted using their errors, was fitted to our CDW models by varying the ionic displacements $\{\mathbf{u}_j\}$ to minimise χ^2 . Further details are in the Supplementary Information.

Acknowledgements

We thank Martin Long and Radu Coldea for very helpful discussions and the UK EPSRC for funding under grant numbers EP/J016977/1 (EB, EMF & ATH) and EP/J015423/1 (SMH). JC wishes to thank the Swiss National Science Foundation for support. NBC was supported by the Danish Agency for Science, Technology and Innovation under DANSCATT. Sample preparation was funded through NSERC and the Canadian Institute for Advanced Research. Work at Brookhaven is supported by the Office of Basic Energy Sciences (BES), Division of Materials Science and Engineering, U.S. Department of Energy

(DOE), under Contract No. DE-AC02-98CH10886. We thank U. Ruett and D. Robinson for invaluable assistance with complementary higher energy measurements performed at P07, DESY & 6-ID-D, APS. Use of the Advanced Photon Source, an Office of Science User Facility operated for the U.S. DOE Office of Science by Argonne National Laboratory, was supported by the U.S. DOE under Contract No. DE-AC02-06CH11357.

Author Contributions

EB, JC, EMF, SMH & ATH carried out the experiments with important input from beamline scientists LB & SDB. Analysis of results was carried out by EB, JC, EMF, SMH & ATH; AB created the program that fitted the intensities to the ionic displacements. NBC, MH & MvZ contributed additional measurements at high energy. DB, WH & RL supplied samples. All authors contributed to the manuscript.

References

1. Tranquada, J. M. Stripes and superconductivity in cuprates. *Physica B: Condensed Matter* **407**, 1771-1774 (2012).
2. Doiron-Leyraud, N. *et al.* Quantum oscillations and the Fermi surface in an underdoped high- T_c superconductor. *Nature* **447**, 565-568 (2007).
3. Chang, J. *et al.* Nernst and Seebeck coefficients of the cuprate superconductor $\text{YBa}_2\text{Cu}_3\text{O}_{6.67}$: a study of Fermi surface reconstruction. *Phys. Rev. Lett.* **104**, 057005 (2010).
4. Wu, T. *et al.*, Magnetic-field-induced charge-stripe order in the high temperature superconductor $\text{YBa}_2\text{Cu}_3\text{O}_y$. *Nature* **477**, 191–194 (2011).
5. Ghiringhelli, G. *et al.* Long-Range Incommensurate Charge Fluctuations in $(\text{Y,Nd})\text{Ba}_2\text{Cu}_3\text{O}_{6+x}$. *Science* **337**, 821-825 (2012).
6. Achkar, A.J. *et al.*, Distinct Charge Orders in the Planes and Chains of Ortho-III-Ordered $\text{YBa}_2\text{Cu}_3\text{O}_{6+\delta}$ Superconductors Identified by Resonant Elastic X-ray Scattering. *Phys. Rev. Lett.* **109**, 167001 (2012).
7. Blanco-Canosa, S. *et al.* Momentum-Dependent Charge Correlations in $\text{YBa}_2\text{Cu}_3\text{O}_{6+x}$ Superconductors Probed by Resonant X-ray Scattering: Evidence for Three Competing Phases. *Phys. Rev. Lett.* **110**, 187001 (2013).
8. Blanco-Canosa, S. *et al.* Resonant X-ray scattering study of charge-density wave correlations in $\text{YBa}_2\text{Cu}_3\text{O}_{6+x}$. *Phys. Rev. B* **90**, 054513 (2014).
9. Chang, J. *et al.* Direct observation of competition between superconductivity and charge density wave order in $\text{YBa}_2\text{Cu}_3\text{O}_{6.67}$. *Nature Physics* **8**, 871-876 (2012).
10. Blackburn, E. *et al.* X-ray Diffraction Observations of a Charge-Density-Wave Order in Superconducting Ortho-II $\text{YBa}_2\text{Cu}_3\text{O}_{6.54}$ Single Crystals in Zero Magnetic Field. *Phys. Rev. Lett.* **110**, 137004 (2013).

11. Huecker, M *et al.* Competing charge, spin, and superconducting orders in underdoped YBaCuO_y. *Phys. Rev. B* **90**, 054514 (2014).
12. Monceau, P. Electronic crystals: an experimental overview. *Adv. Phys.* **61**, 325 (2012).
13. Wilson, J., Di Salvo, F. and Mahajan, S. Charge-density waves and superlattices in the metallic layered transition metal dichalcogenides. *Adv. Phys.* **24**, 117 (1975).
14. Zhu, X., Cao, Y., Zhang, J., Plummer, E. W. and Guo, J. Classification of charge density waves based on their nature. *Proc. Nat. Acad. Sci.* **112**, 2367-2371 (2015).
15. Comin, R. *et al.* Charge Order Driven by Fermi-Arc Instability in Bi₂Sr_{2-x}La_xCuO_{6+d}. *Science* **343**, 390, (2014).
16. da Silva Neto *et al.* Ubiquitous Interplay Between Charge Ordering and High-Temperature Superconductivity in Cuprates. *Science* **343**, 393-396 (2014).
17. Hashimoto, M. *et al.* Direct observation of bulk charge modulations in optimally doped Bi_{1.5}Pb_{0.6}Sr_{1.54}CaCu₂O_{8+d}. *Phys. Rev. B* **89**, 220511 (2014).
18. Thampy, V. *et al.* Rotated stripe order and its competition with superconductivity in La_{1.88}Sr_{0.12}CuO₄. *Phys. Rev. B* **90**, 100510 (2014).
19. Tabis, W. *et al.* Charge order and its connection with Fermi-liquid charge transport in a pristine high-*T_c* cuprate. *Nature Communications* **5**, 5875 (2014).
20. Christensen, N. B. *et al.* Bulk charge stripe order competing with superconductivity in La_{2-x}Sr_xCuO₄ (*x*=0.12). Preprint at <http://arxiv.org/abs/1404.3192> (2014).
21. Croft, T. P., Lester, C., Senn, M. S., Bombardi, A. and Hayden, S. M. Charge density wave fluctuations in La_{2-x}Sr_xCuO₄ and their competition with superconductivity. *Phys. Rev. B* **89**, 224513 (2014).

22. Comin, R. *et al.* The symmetry of charge order in cuprates. Preprint at <http://arxiv.org/abs/1402.5415> (2014).
23. Sachdev, S. and La Placa, R. Bond order in two-dimensional metals with antiferromagnetic exchange interactions. *Phys. Rev Lett.* **111**, 027202 (2013).
24. Fujita, K. *et al.* Simultaneous Transitions in Cuprate Momentum-Space Topology and Electronic Symmetry Breaking. *Science* **344**, 612-616 (2014).
25. Achkar, A. J. *et al.* Orbital symmetry of charge density wave order in $\text{La}_{1.875}\text{Ba}_{0.125}\text{CuO}_4$ and $\text{YBa}_2\text{Cu}_3\text{O}_{6.67}$. Preprint at <http://arxiv.org/abs/1409.6787> (2014).
26. Wang, Y. and Chubukov, A. Charge-density-wave order with momentum $(2Q,0)$ and $(0,2Q)$ within the spin-fermion model: Continuous and discrete symmetry breaking, pre-emptive composite order, and relation to pseudogap in hole-doped cuprates. *Phys. Rev. B* **90**, 035149 (2014)
27. LeBoeuf, D. *et al.*, Thermodynamic phase diagram of static charge order in underdoped $\text{YBa}_2\text{Cu}_3\text{O}_y$. *Nature Physics* **9**, 79–83 (2013).
28. Doiron-Leyraud, N. *et al.*, Evidence for a small hole pocket in the Fermi surface of underdoped $\text{YBa}_2\text{Cu}_3\text{O}_y$. *Nature Communications* **6**, 6034 (2015).
29. Sebastian, S. E. *et al.* Normal-state nodal electronic structure in underdoped high- T_c copper oxides. *Nature* **511**, 61–64 (2014).
30. Comin, R. *et al.* Broken translational and rotational symmetry via charge stripe order in underdoped $\text{YBa}_2\text{Cu}_3\text{O}_{6+y}$. *Science* **347**, 1335-1339 (2015).
31. Campbell, B. J., Stokes, H. T., Tanner, D. E. and Hatch, D. M. ISODISPLACE: An Internet Tool for Exploring Structural Distortions. *J. Appl. Cryst.* **39**, 607-614 (2006).
32. Raichle, M. *et al.*, Highly Anisotropic Anomaly in the Dispersion of the Copper-Oxygen Bond-Bending Phonon in Superconducting $\text{YBa}_2\text{Cu}_3\text{O}_7$ from Inelastic Neutron Scattering. *Phys. Rev. Lett.* **107**, 177004 (2011).

33. Först, M. *et al.* Femtosecond x rays link melting of charge-density wave correlations and light-enhanced coherent transport in $\text{YBa}_2\text{Cu}_3\text{O}_{6.6}$. *Phys. Rev. B* **90**, 184514 (2014).
34. Briffa, A., Forgan, E. M., Blackburn, E., Hayden, S. M. and Long, M. W. The Reconstruction of the Fermi Surface in Under-doped $\text{YBa}_2\text{Cu}_3\text{O}_{6.54}$ by Charge Density Waves and the Effects on Quantum Oscillations *in preparation* (2015).
35. Allais, A., Chowdhury, D. and Sachdev, S. Connecting high-field quantum oscillations to the pseudogap in the underdoped cuprates. *Nature Communications* **5**, 5771 (2014).

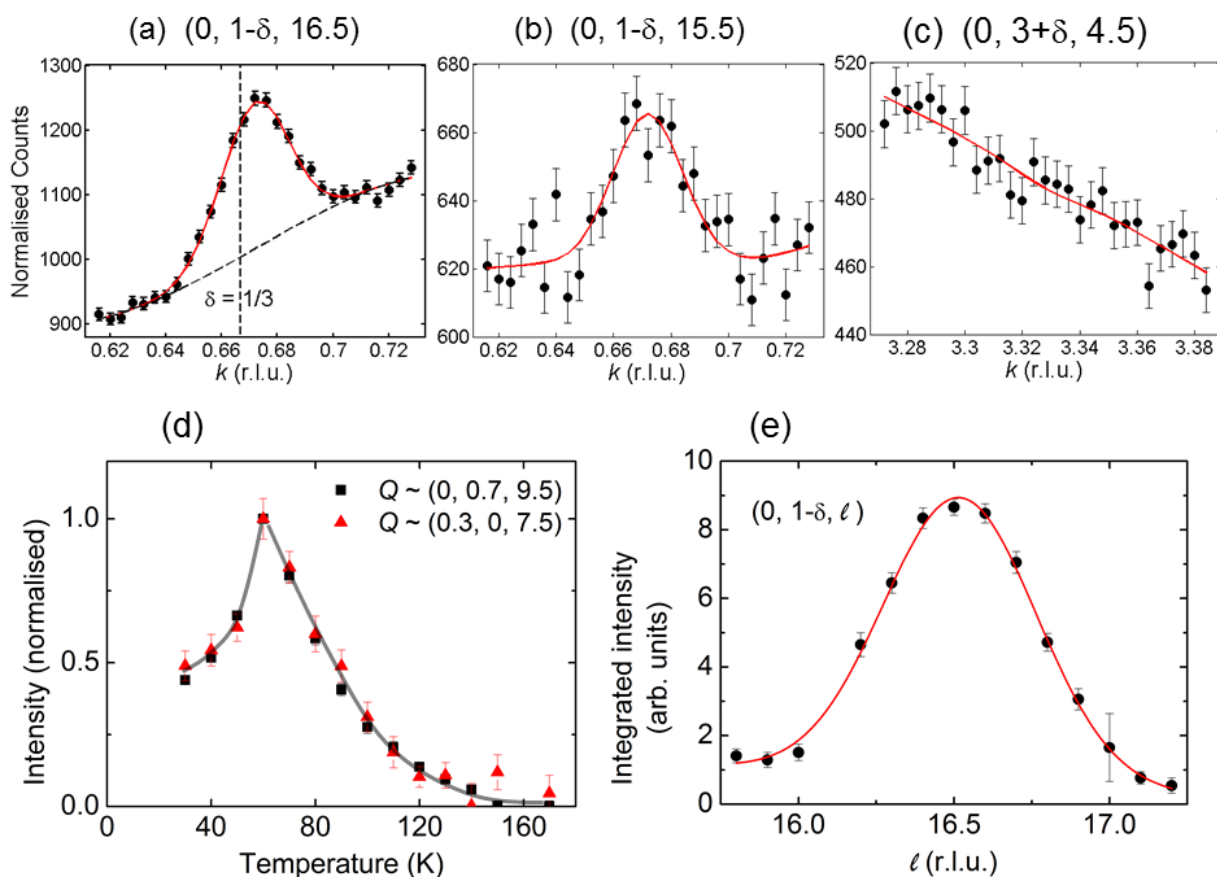


Figure 1: Typical observations of CDW satellites at 60 K and their temperature-dependence

(a)-(c) are obtained from the CDW with modulation vector \mathbf{q}_b . The counts are normalised so that they are approximately per second, measured over 10 s per point, plotted versus wavevector along the \mathbf{b}^* direction k . (a) shows a strong satellite, along with the fit line which gives the intensity as the area under the peak. The CDW is clearly centred at an incommensurate position ($\delta_b \sim 0.328$), although the value $1/3$ lies within the peak. (b) shows a weaker peak, and (c) is taken at a position where the CDW signal is unobservably small, and the fitted area of the peak is controlled by Poisson errors. (d) The intensities of CDW satellites for both \mathbf{q}_a ($\delta_a \sim 0.323$) and \mathbf{q}_b ($\delta_b \sim 0.328$) modes, normalised to their intensities at T_c , are plotted versus temperature; these track each other within errors. (e) The integrated intensity of the satellite (a) is plotted versus ℓ . The width in ℓ , which reflects the finite c -axis coherence of the CDW, is much larger than the instrument resolution. Since it is a property of the CDW, it is the same for all satellites.

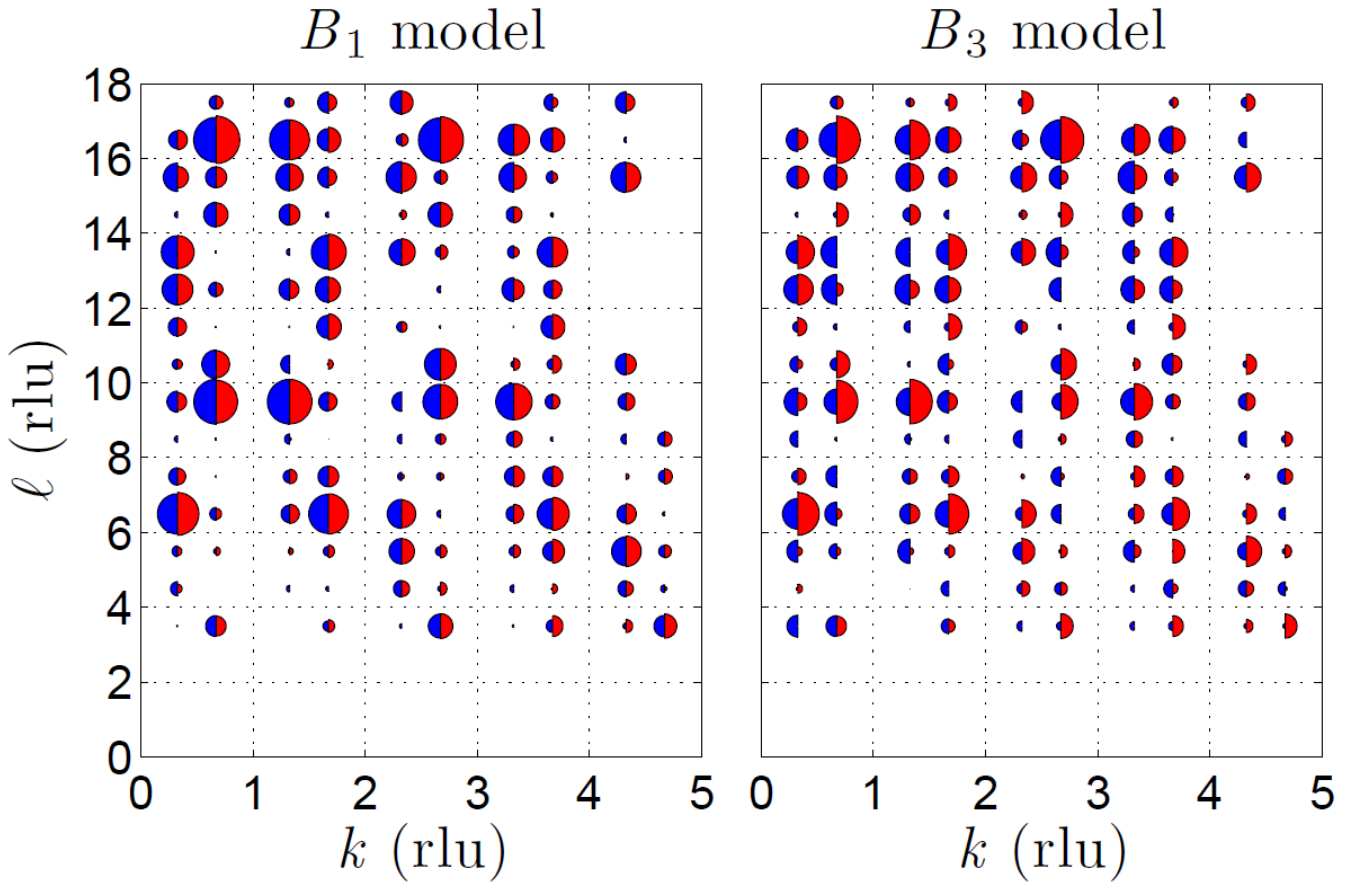


Figure 2: Typical data compared with the fits to two possible models.

This shows a map of the measured satellite intensities in the $(0, k, \ell)$ plane of reciprocal space for the CDW with modulation \mathbf{q}_b . The measured intensities are proportional to the areas of the red semicircles on the right of each \mathbf{Q} -point. The blue semicircles show the results of two different fits, to models described later in the text. Blank spaces indicate inaccessible regions or where a spurious signal prevented measurements of the CDW order. Further intensity maps, including those for the \mathbf{q}_a mode are given in Supplementary Information.

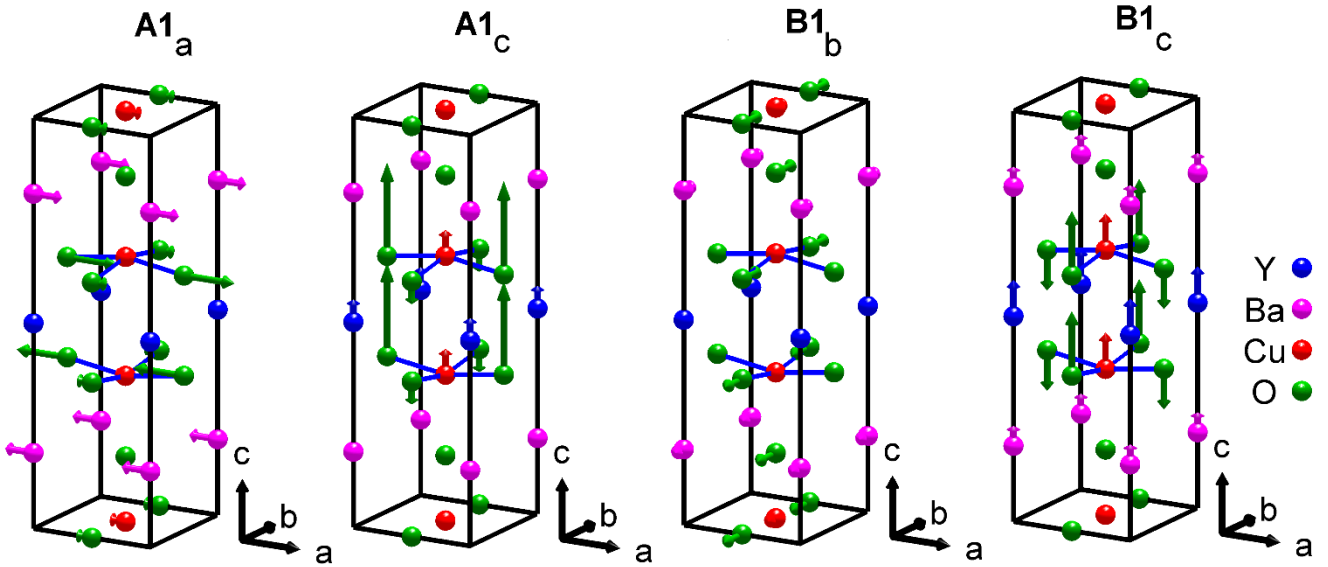


Figure 3: Representation of the CDW ionic displacement motifs (exaggerated) for an unmodulated unit cell

These are shown separately for the \mathbf{q}_a and \mathbf{q}_b modes of the CDW. The basal plane and c -axis displacements have a $\pi/2$ phase difference and hence are shown in separate unit cells. The next crystal unit cells in the c -direction would be in antiphase with those shown here. The oxygen sites in the CuO chains represented here are half-occupied in our sample.

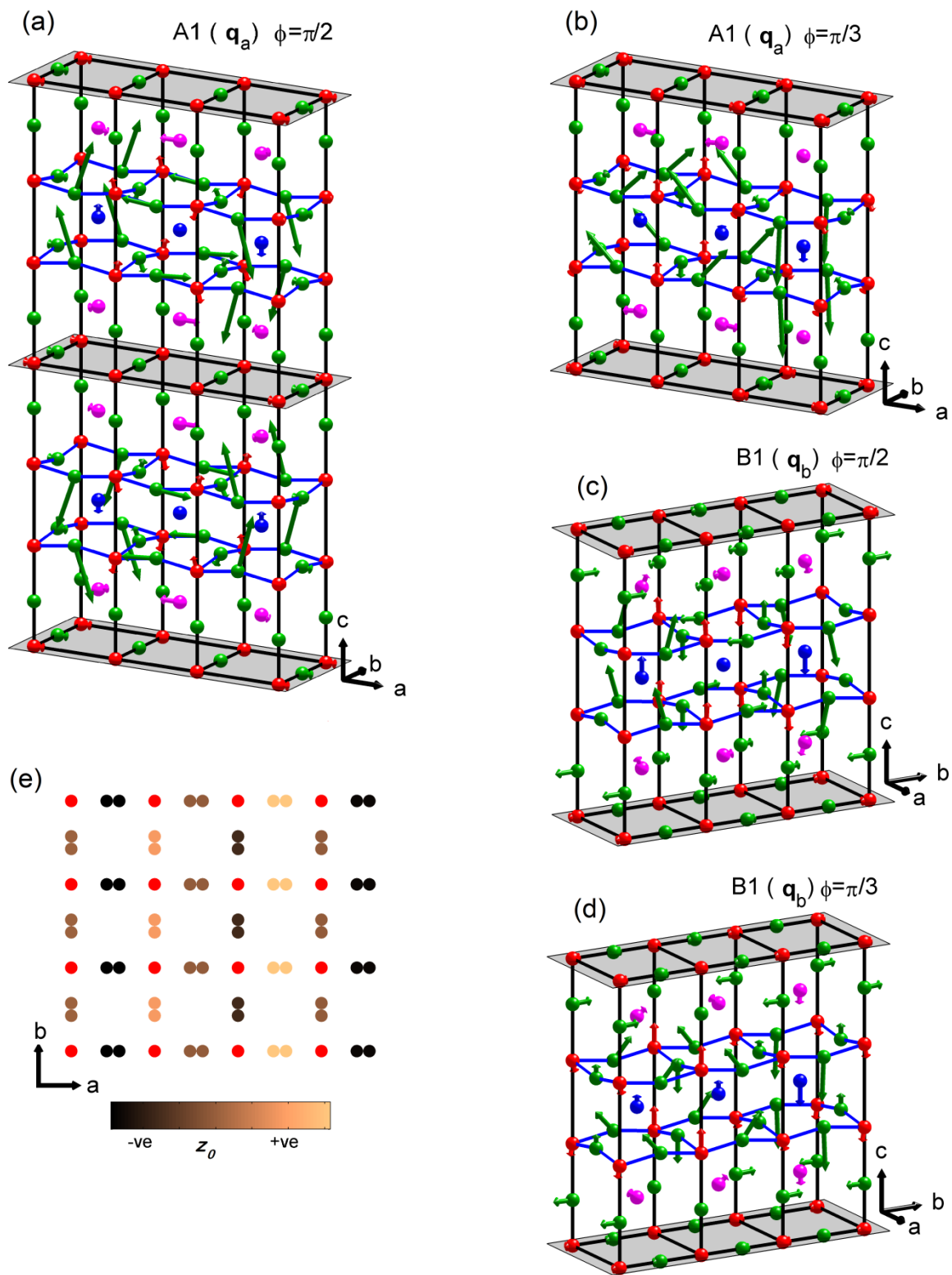


Figure 4: Representation of modulated ionic displacements (exaggerated) for both CDW modes.

The shaded planes passing through the CuO chain layers are the mirror planes of the CDWs, as may be recognised in panel (a). In panels (a) – (d), the two CDW modes are shown with two of the possible phases of the modulation relative to the crystal lattice. Note that in one case the yttrium z -displacements in adjacent cells along the modulation direction are +, 0, -, and in the other case +, +, 2-. The total displacement of the ions in the crystal is expected to be the sum of those associated with the \mathbf{q}_a and \mathbf{q}_b modulation vectors. In panel (e) is a representation of the spatial variation of the difference z_0 of the bilayer oxygen displacements in the z -direction, shown for one (\mathbf{q}_a) of two modulation directions present in the crystal. It has the same symmetry as a “bond d -density wave” along the δ_a direction..

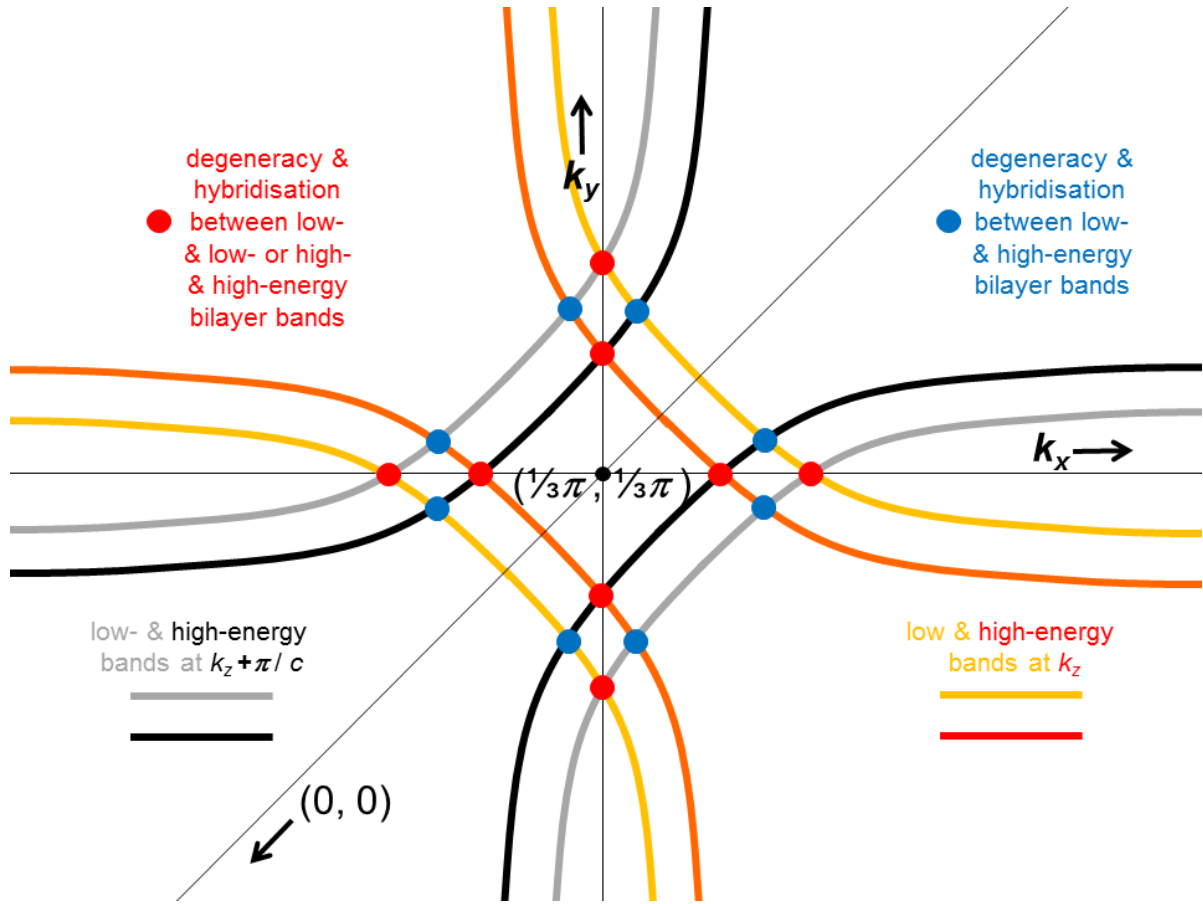


Figure 5: Effects of the CDW on the hybridisation of the CuO_2 bilayer electron states.

The figure shows schematically a corner of the Brillouin zone (BZ) with the two bands for the CuO_2 bilayer at a given k_z in red and orange respectively. The effects of a 2- \mathbf{q} CDW, which we represent with commensurate δ of $\frac{1}{3}$, is to add additional zone boundaries and to allow hybridisation with the same bands, translated from the other corners of the BZ at $k_z + \pi/c$ (grey and black) and k_z (red and orange). In principle these bands should be in slightly different positions to represent the k_z dispersion of the bands. The positions where these states are degenerate and hybridisation may occur to create small electron-like sheets are marked with red and blue dots.